Polymer Communication

Residual stress effect on degradation of polyimide under simulated hypervelocity space debris and atomic oxygen

Ronen Verker [a,b,*], Eitan Grossman [a], Irina Gouzman [a], Noam Eliaz [b]

[a] *Space Environment Section, Soreq NRC, Yavne 81800, Israel*
[b] *Department of Solid Mechanics, Materials and Systems, Tel-Aviv University, Ramat Aviv, Tel-Aviv 69978, Israel*

Abstract

Polyimides are used as the outer layer of thermal control insulation blankets covering most of the external spacecraft surfaces that are exposed to space environment. The combined effect of ground simulated hypervelocity space debris impacts and atomic oxygen (AO) on the fracture of polyimide films was studied. A laser-driven flyer system was used to accelerate aluminum flyers to impact velocities of up to 3 km/s. The impacted films were exposed to an RF plasma source, which was used to simulate the effect of AO in the low Earth orbit. Scanning electron microscopy and atomic force microscopy were used to characterize the fracture and surface morphology. When exposed to oxygen RF plasma, the impacted polyimide film revealed a large increase in the erosion rate, the damage being characterized mainly by the formation of new holes. This effect is explained by the formation of residual stresses due to the impact and enhancement of oxygen diffusivity and accumulation. A complementary experiment, in which a stressed polyimide was exposed to RF plasma, supports this model. This study demonstrates a synergistic effect of the space environment components on polymers' degradation, which is essential for understanding the potential hazards of ultrahigh velocity impacts and AO erosion for completing a successful spacecraft mission.
© 2006 Elsevier Ltd. All rights reserved.

Keywords: Polyimide; Atomic oxygen; Space debris

1. Introduction

Nowadays, numerous satellites are being launched into low Earth orbit (LEO) altitudes, ranging from 200 to 800 km. Natural and man-made LEO space environment possesses many obstacles to a successful spacecraft mission. The degrading environment for polymers includes atomic oxygen (AO), ultraviolet (UV) and ionizing radiation, ultrahigh vacuum (UHV), thermal cycles, micrometeoroids and orbital debris [1,2]. Due to separate, combined or synergistic interactions with these space hazards, polymers in particular suffer a relatively rapid erosion, chemical and structural modification, and surface roughening. This might lead to irreversible degradation of optical, thermal, electrical and mechanical properties [3–5].

Atomic oxygen, produced by the photo-dissociation of molecular oxygen in the upper atmosphere, is the main constituent of the residual atmosphere in LEO [6]. AO is considered as one of the most serious hazards to spacecraft external materials. Although the oxygen atoms have low density ($\sim 1 \times 10^8$ atoms/cm^3) and low energy (~ 0.1 eV), their collision with the external surfaces of space vehicles, orbiting at a velocity of 8 km/s, results in impacts equivalent to an energy of ~ 5 eV and flux of 10^{14}–10^{15} O-atoms/(cm^2 s) [7–9].

Hypervelocity debris at LEO altitudes are man-made constituents, originating from large objects such as spent satellites and rockets, and consisting mostly of small objects such as aluminum oxide fuel particles, paint chips and fragmentation objects from collisions of these bodies in orbit [7,10]. Typical velocities of debris particles range from a few kilometers per

second up to 16 km/s, making these hypervelocity particles a threat to spacecraft [11,12].

Polyimide films are widely used onboard spacecraft, mainly as external thermal blankets [12]. Hence, they are exposed extensively to AO as well as to debris impacts. Numerous efforts have been made to protect these external thermal blankets from AO, mainly by the use of protective layers. However, the effect of AO erosion on polyimide surfaces already fractured by hypervelocity debris has not yet been studied. In this work, the effect of combined hypervelocity impacts and RF plasma simulated AO on the fracture of polyimide films was studied. The mechanism of the revealed synergistic degradation effect is discussed.

2. Experimental section

The material studied in this work was oxydianiline–pyromellitic dianhydride (ODA–PMDA) polyimide (Pyre-M.L. RC-5019 by Industrial Summit Technology, Co.). Thin polyimide films, 25–30 μm-thick, were produced at a bench-scale process by casting a pre-mixed solution of ODA–PMDA in *N*-methyl-pyrrolidone on a BK7 glass window imbedded in a stainless steel mold [13,14]. The curing conditions used were similar to the process developed by DuPont, Inc. [15]. The ODA–PMDA polyamic acid was heated to 200 °C in air at a ramp rate of 4 °C/min and held for a period of 30 min, then heated to 350 °C in the presence of pure nitrogen at a ramp rate of 2 °C/min and held for a period of 60 min. In order to avoid residual stresses, the final stage was slow cooling at a ramp rate of 2 °C/min down to room temperature.

The laser-driven flyer (LDF) method was used for generating simulated space hypervelocity debris with dimensions ranging from 10 to 100s of micrometers and velocities of up to 3 km/s [16–18]. The experimental set-up and flyer velocity measurements have been described in details elsewhere [19]. The Soreq's LDF system is based on a high-power titanium:sapphire laser (Thales Laser) with a wavelength of 810 nm, pulse energies from 250 to 710 mJ, and pulse length of 300 ps. The laser beam is guided through a set of mirrors into a vacuum chamber operating at a base pressure of 65 mTorr. Before entering the chamber, the beam passes through a focusing lens attached to a linear motion mechanism. Inside the chamber, the laser beam irradiates a 12 μm-thick pure aluminum foil through a BK7 glass substrate. The aluminum foil was bonded to the BK7 glass using a field-assisted diffusion bonding process. The beam passes through the glass without interacting with it, until it hits the aluminum/glass interface. At the interface, a high-temperature and high-pressure plasma is formed, which then expands perpendicularly to the foil. The expanding plasma induces a series of shock and rarefaction waves, forming a spall [20]. A pressure gradient between the high-pressure plasma on one side of the spall and the low-pressure vacuum on the other side of the spall causes the spalled layer acceleration, resulting in an aluminum layer, 1 mm in diameter, flying away at ultrahigh velocity of up to about 3 km/s. The accelerated aluminum layer is composed of small flyers, each of the order of few tens

of micrometers in size, all traveling at ultrahigh velocities. A continuous He:Ne laser beam was set orthogonal to the flyer's trajectory, and by using a prism the beam crosses the flyer's path twice. The two parallel beams were set at a distance of 13 mm from each other. A photodiode attached to an oscilloscope receives the continuous laser signal. As the flyer crosses and blocks the continuous laser's path, two peaks are detected by the oscilloscope, allowing the velocity calculation.

A conventional RF plasma reactor (15 W, 13.56 MHz, Model PDC-3XG from Harrick), operating at 500 mTorr of air, was used to simulate the effect of AO in the low Earth orbit [21,22]. Samples were located 150 mm downstream from the reactor, in the afterglow region where they are exposed to a mixture of atomic and molecular oxygen, excited species and vacuum UV (VUV) radiation. Nevertheless, the contribution of ions, VUV and excited species is reduced compared to the RF plasma reactor environment [21,23]. Although LEO AO is hyperthermal, the RF plasma environment with thermal AO is considered a useful tool for materials' evaluation. The space equivalent AO flux at the sample's position was 2.4×10^{14} O-atoms/(cm^2 s). AO equivalent fluence measurements were conducted based on 25 μm-thick Kapton-HN film (DuPont, Inc.) mass loss, assuming an erosion yield of 3×10^{-24} cm^3/O-atoms [24]. The erosion yield was determined gravimetrically, using an analytical balance (Model UM3 from Mettler) with an accuracy of ± 1 μg.

The morphology of fractured surfaces, resulting from the hypervelocity impacts, was studied using an environmental SEM (ESEM, Model Quanta 200 from FEI). The morphology of RF plasma-exposed samples was studied using an atomic force microscope (AFM, Nanoscope IV MultiMode from Veeco).

3. Results and discussion

Fig. 1a and b shows a 24 μm-thick polyimide film, impacted by 2.4 km/s flyers before and after exposure to 2.6×10^{20} O-atom/cm^2 AO equivalent fluence, respectively. The ESEM images were taken from the impact exit side.

The impacted polyimide sample (Fig. 1a) is characterized by two minor radial cracks formed around the central impact zone. These short radial cracks developed as a secondary process, after pieces of polyimide were sheared-off from the central impact zone. As for the RF plasma exposure of the polyimide sample (Fig. 1b), significant erosion is apparent mostly by expansion of holes, formed by the ultrahigh velocity impact, and surprisingly, extensive erosion apparent by the formation of a large number of new holes. These new holes tend to form in a radial star-like pattern around the sample's central impact zone. It is suggested that due to the ultrahigh velocity impact, a residual tensile stress field is developed within the polyimide film in radial directions, leading to the formation of the new holes in a star-like pattern.

A model is proposed to explain the extensive erosion and the formation of the new macro-holes in the impacted polyimide film due to UV and AO exposures in the RF plasma
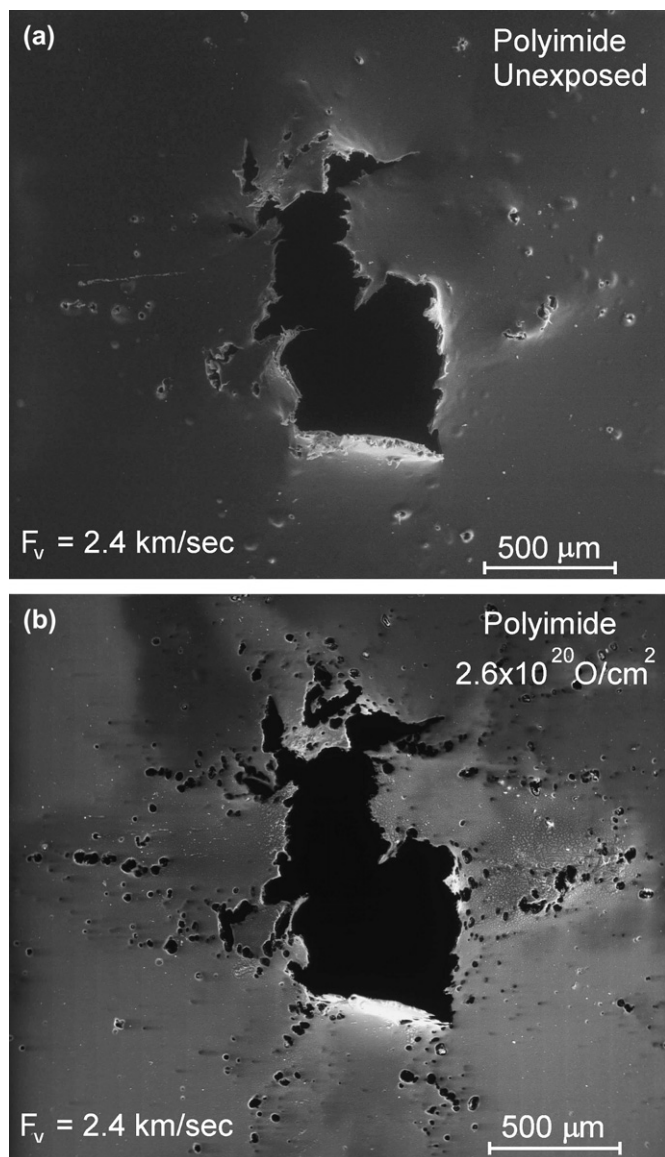
Fig. 1. ESEM images of polyimide film (24 μm-thick), impacted by 2.4 km/s flyers (a), and the same impacted polyimide film subsequently exposed to AO equivalent fluence of 2.6×10^{20} O-atoms/cm² (b).

afterglow. The new macro-hole formation is a result of a multi-step process:

(i) Establishment of a field of residual tensile stresses within the polymer due to the ultrahigh velocity impacts and temporary local increase in the average temperature, to values that may exceed the glass transition temperature [19].

(ii) Increase in the polymer's local free volume (i.e. the volume that is not occupied by the polymer chains), in regions of higher residual tensile stress and/or higher average temperature [25].

(iii) Increased oxygen diffusion into the polymer due to residual tensile stresses that reduce the local chemical potential. It is well known that diffusion processes can be motivated by gradients of stress, temperature and/or electrical potential. An elastic tensile stress decreases the chemical potential of an interstitial solute. This is true whether the elastic stress is externally applied or is residual. Since the gradient of chemical potential is the fundamental driving force for diffusion, the flux of solute is:

$$J = -Bc\frac{\partial \mu}{\partial c}\nabla c = -D\nabla c + \frac{Dc\overline{V}_{sol}}{kT}\nabla(\sigma_{h}), \qquad (1)$$

where B is the mobility, c concentration, μ chemical potential, D diffusivity, $\overline{V}_{sol}$ partial molal volume of the solute atom in the material, k Boltzmann constant, T temperature, and σ_{h} hydrostatic component of the elastic stress field [26,27]. The situation is even more complex in the case of the polyimide samples studied here. Not only does the ultrahigh velocity impact establishes a field of residual tensile stresses, the local free volume is also increased (for the amorphous phase – as long as the stress is not high enough to induce ordering of the polymer chains and crystallization). It is agreed that the polymer fractional free volume has a major effect on the diffusivity and permeability of AO [25]. Furthermore, oxygen diffusion, which is the rate-limiting step in many photo-oxidative reactions [28,29], can be affected by other factors, such as polymer crystallinity, cross-linking and morphology. The latter is a parameter that has an important influence on the rate of polymer photochemical degradation. Micro-cracks, initially developed on the surface at stressed regions, facilitate the diffusion of oxygen into the bulk [28].

(iv) Local increase in the AO-induced erosion rate. In general, AO reaction with polymers is a thermally activated, two-step process. In the first step, AO diffuses into the polymer. In the second step, the AO reacts more readily with the weaker polymer bonds [30]. The reaction's volatile products (i.e. H_2O, CO and CO_2) then diffuse towards the film surface and desorb. One of the effects of the stress is to decrease the efficiency of recombination of photochemically generated radical pairs, by increasing the separation between them. Consequently, the probability of radical trapping and radical-dependent reactions is increased. This leads to an increased rate of degradation, which first takes place on the polymer's surface, thus affecting its morphology, followed by bulk etching [28].

(v) Formation of new macro-holes, which replicate the distribution of residual tensile stresses.

In order to verify the suggested model, the following experiment was carried out. Fig. 2a shows a schematic presentation of RF plasma exposure set-up of a 24 μm-thick and 10 mm wide polyimide film that is stressed by a cone-shaped pin (tip diameter ∼660 μm), which is connected to a pre-stressed spring (spring constant $k = 219.2$ N/m, spring displacement in the stressed condition $\Delta x = 3.5$ mm). The polyimide film was strictly bound to the bottom side of the base plate. It
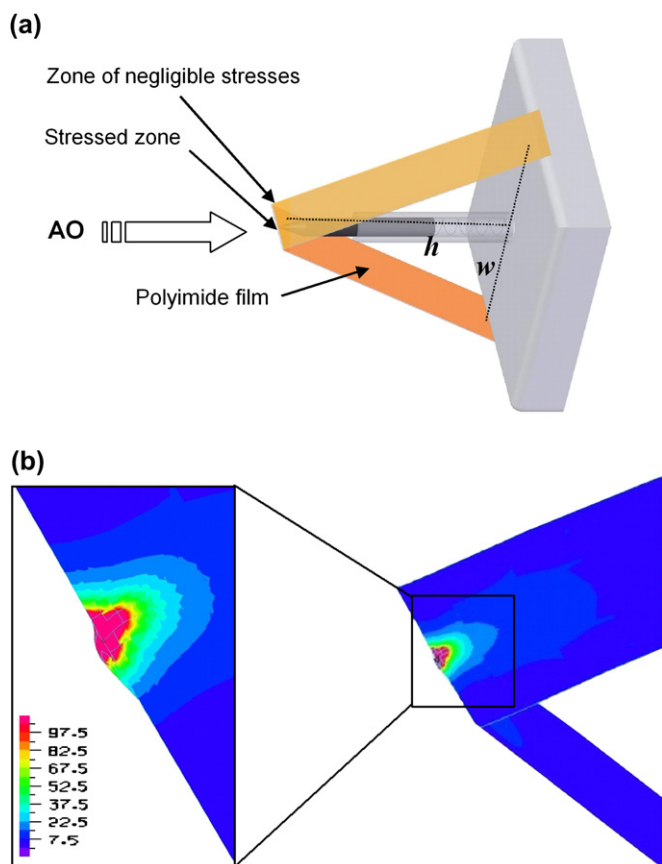
(a)

(b)

Fig. 2. (a) Schematic presentation of RF plasma exposure set-up of a stressed polyimide film. Height of spring in the pre-stressed condition $h = 35.3$ mm, base of imaginary triangle $w = 40.2$ mm. (b) Finite element analysis of the von Mises (effective) stress — illustrating the significant decrease in stress along the film apex as the distance from the contact loading increases. The color scale is in MPa (For interpretation of the references to color in this figure legend, the reader is referred to the web version of this article).

was hypothesized that this local loading should result in the establishment of stress distribution inside the polymer, with stress values that are considerably higher around the contact points, and negligible stress values near the two longitudinal sides of the film. Finite element analysis was carried out in order to justify this hypothesis and support the establishment of stress distribution inside the polymer while under stress. The analysis was carried out on Kapton-HN polyimide (Young's modulus $E = 2.94$ GPa, Poisson's ratio $\nu = 0.34$) under plane strain conditions, applying a quasi-static model, a linear elastic approximation and contact elements in a commercial finite element code, ADINA version AUI 8.3.1. The resulting distribution of effective stress in the z-direction is presented in Fig. 2b. The stress values around the contact area were higher than 60 MPa. This stress level is within the plastic regime of the studied polyimide, as obtained by tensile stress measurements performed in accordance with ASTM D 882-88 Standard [31]. It is evident that the stress level near the two longitudinal sides of the film is negligible compared to the stress level around the central contact area. The related image of the strain field (not shown herein) also indicated plastic deformation around the contact area. These numerical results

were supported by macroscopic inspection of the sample right after the experiment, from which it was clear that the sample was deformed plastically only around the region of contact.

The stressed polyimide film was exposed to 1.6×10^{20} O-atoms/cm^2 AO equivalent fluence. After exposure, the surface morphology was investigated by AFM in two different zones — one close to the longitudinal edge of the film where only negligible effective stresses could be developed, and the other close to the center, where fairly high stresses were developed. The corresponding representative images (out of 4–6 images taken for each zone) are shown in Fig. 3b and c, respectively. Fig. 3a shows AFM morphology of the pristine polyimide. All images are 5×5 μm size and have a z-range of 100 nm. For each of the images the root mean square (RMS) roughness, R_q (averaged over several images), is given. The RMS roughness is defined as follows:

$$R_q = \sqrt{\frac{\sum (Z_i - Z_{ave})^2}{N}}, \tag{2}$$

where Z_{ave} is the average Z height value within a given area, Z_i is the current Z value and N is the number of points within the given area.

Pristine polyimide (Fig. 3a) is characterized by a smooth surface, having RMS roughness of 1.2 nm. Following RF plasma exposure, each of the two zones of the stressed polyimide film is characterized by a different surface morphology. The negligibly stressed zone (Fig. 3b) shows a carpet-like morphology, which is typical for erosion of polyimide by AO [32], and an RMS roughness of 4.5 nm. The morphology of the stressed zone (Fig. 3c), on the other hand, is characterized by rough and unordered surface with an RMS roughness of about 16.9 nm. The increased roughness is a result of a combined effect of stress and AO attack.

In order to strengthen this conclusion, a reference sample was also stressed by the set-up shown in Fig. 2a for the same duration as for the RF plasma exposure test (185 h). AFM analysis (images not shown) proved that the surface morphology of this control sample did not change along the film apex, i.e. the effect demonstrated in Fig. 3 is not due to stress per se. These results further support the model for new macro-hole formation due to AO erosion, which follows the distribution of residual tensile stresses and local free volume, as previously discussed. Summarizing in brief, local tensile stresses accompanied by an increase in the local free volume facilitated the diffusion of oxygen into the polymer, thus leading to enhanced degradation and formation of rough, unordered surface morphology. At the same time, in negligibly stressed regions (less than 5 mm away), uniform surface erosion occurred.

4. Conclusions

Individual and synergistic effects of ultrahigh velocity impacts and RF plasma exposure on polyimide films were studied. A synergistic erosion effect was observed after
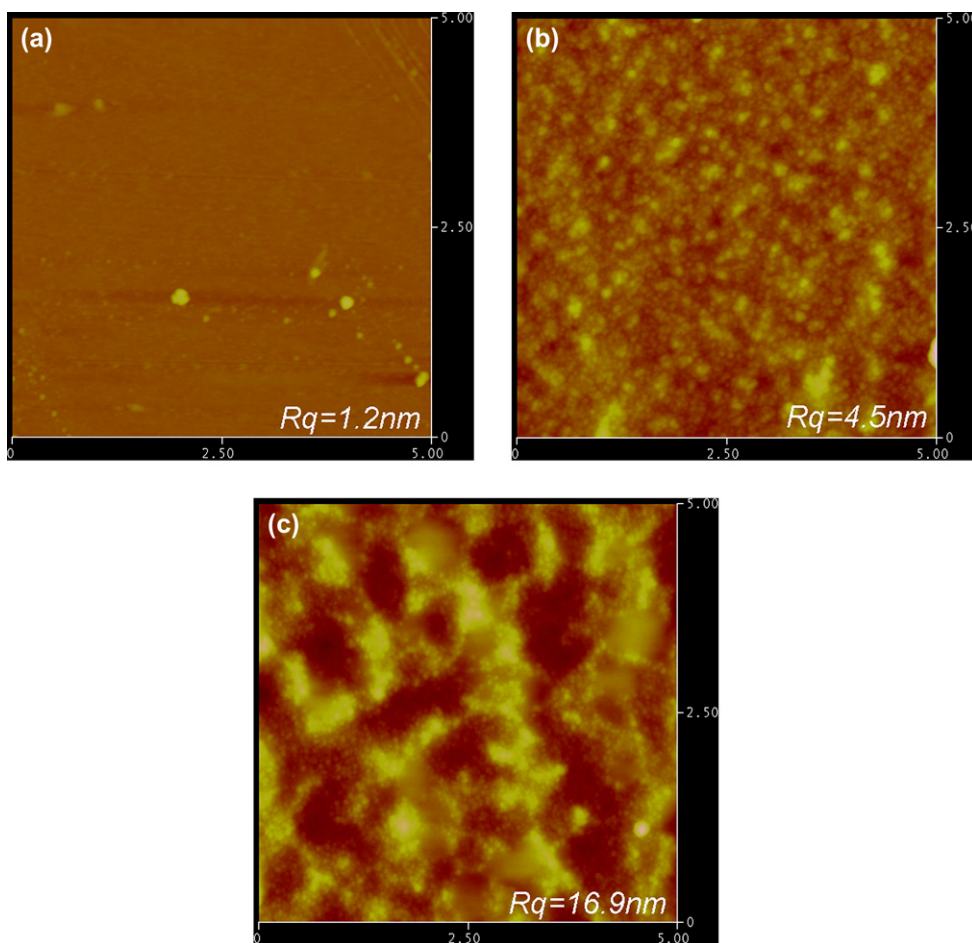
Fig. 3. AFM image of a pristine polyimide film (a). AFM images of negligibly stressed (b) and stressed (c) zones of polyimide film after exposure to 1.6×10^{20} O-atoms/cm^2 equivalent AO fluence. Scan size 5×5 μm; z-range: 100 nm.

hypervelocity impact and subsequent RF plasma exposure of polyimide films. The accelerated erosion of the polyimide sample is characterized mainly by the formation of RF plasma-induced new macro-holes. These holes tend to be formed in a radial star-like pattern around the sample's central impact zone. A model was suggested to explain this phenomenon, based on the introduction of residual tensile stresses in a star-like pattern around the impacted area. These residual stresses generate a local increase in the polymer free volume, which facilitates oxygen diffusion into the polymer, thus initiating the process of local high-rate degradation.

This study elucidates the synergistic effect of two important components of space environment on the erosion of polymers. Its outcomes are essential for understanding the potential hazards of ultrahigh velocity impacts and AO erosion on the probability for completing a successful spacecraft mission.

Acknowledgements

References

[1] Tribble AC. The space environment: implementation for spacecraft design. Princeton, New Jersey: Princeton University Press; 1995.
[2] Bedingfield KL, Leach RD, Alexander MB. NASA Reference Publication 1390; 1996.
[3] Grossman E, Gouzman I. Nuclear Instruments and Methods in Physics Research Section B − Beam Interactions with Materials and Atoms 2003;208:48−57.
[4] Grossman E, Gouzman I, Viel-Inguimbert V, Dinguirard M. Journal of Spacecraft and Rockets 2003;40:110−3.
[5] Houdayer A, Cerny G, KlembergSapieha JE, Czeremuszkin G, Wertheimer MR. Nuclear Instruments and Methods in Physics Research Section B − Beam Interactions with Materials and Atoms 1997;131:335−40.
[6] Minton TK, Garton DJ. Dynamics of atomic-oxygen-induced polymer degradation in low Earth orbit. In: Dressler RA, editor. Chemical dynamics in extreme environments. Advanced series in physical chemistry. Singapore: World Scientific; 2001. p. 420−89.
[7] Hastings D, Garrett H. Spacecraft−environment interactions. Cambridge: Cambridge University Press; 1996.
[8] Koontz SL, Albyn K, Leger LJ. Journal of Spacecraft and Rockets 1991; 28:315−23.
[9] Reddy RM. Journal of Materials Science 1995;30:281−307.

[10] Tennyson RC, Shortliffe G. In: Paillous A, editor. Seventh international symposium on materials in space environment, ESTEC Noordwijk. The Netherlands: ESA Publication; 1997. p. 485.

[11] Miao J, Stark JPW. Planetary and Space Science 2001;49:927−35.

[12] Silverman EM. Space environmental effects on spacecraft − LEO material selection guide. NASA contractor report no. 4661. Langley Research Center; 1995.

[13] Industrial Summit Technology Co. Technical bulletin #ML-1-95, www. istusa.com.

[14] Hybrid Plastics, Inc. Technical bulletin, http://www.hybridplastics.com/pdf/POSS-Kapton%20PI%20Spec.pdf.

[15] Du-Pont. Inc. Technical bulletin, PYRALIN® Polyimide coating PI 2545 PI 2540 product information; February 1993.

[16] Stein C, Roybal R, Tlomak P. Materials in space environment. In: Proceedings of the ESA eighth international symposium, Arcachon, France; 5−9 June, 2000.

[17] Tighe A, Gabriel S, Van Eesbeek M. Materials in space environment. In: Proceedings of the ESA eighth international symposium, Arcachon, France; 5−9 June, 2000.

[18] Roybal R, Shively J, Stein C, Tolmak P. Cost effective testing for the 21st century. In: Proceedings of the 19th space simulation conference. Baltimore, MD, USA; 29−31 October, 1996.

[19] Verker R, Eliaz N, Gouzman I, Eliezer S, Fraenkel M, Maman S, et al. Acta Materialia 2004;52:5539−49.

[20] Eliezer S. The interaction of high-power lasers with plasmas. Bristol: Institute of Physics; 2002.

[21] Intrater R, Lempert G, Gouzman I, Grossman E, Cohen Y, Rein DM, et al. High Performance Polymers 2004;16:249−66.

[22] Grossman E, Gouzman I, Lempert G, Noter Y, Lifshitz Y. Journal of Spacecraft and Rockets 2004;41:356−9.

[23] Golub MA, Wydeven T. Polymer Degradation Stability 1988;22: 325−38.

[24] ASTM E-2089-00. Standard practices for ground laboratory atomic oxygen interaction evaluation of materials for space applications. In: Annual book of ASTM standards, vol. 15.03. West Conshohocken, PA, USA: ASTM International; 2002. p. 752−6.

[25] Klopffer MH, Flaconneche B. Oil and Gas Science and Technology 2001;56:223−44.

[26] Larche FC, Cahn WJ. Acta Metallurgica 1982;30:1835−45.

[27] Oriani RA. Hydrogen in metals. In: Proceedings of the conference on fundamental aspects of stress corrosion cracking. Houston, Texas: National Association of Corrosion Engineers; 1969. p. 32−50.

[28] Tyler DR. Journal of Macromolecular Science − Polymer Reviews 2004; C44:351−88.

[29] O'donnell JB, White JR. Journal of Materials Science 1994;29:3955.

[30] Whitaker AF, Jang BZ. Journal of Applied Polymer Science 1993;48: 1341−67.

[31] ASTM D 882-88. Standard test methods for tensile properties of thin plastic sheeting. In: Annual book of ASTM standards, vol. 08.01. Philadelphia, PA, USA: ASTM; 1989.

[32] Zhao XH, Shen ZG, Xing Y-S, Ma SL. Journal of Physics D − Applied Physics 2001;34:2308−14.